Research Square

Preprints are preliminary reports that have not undergone peer review.
They should not be considered conclusive, used to inform clinical practice,
or referenced by the media as validated information.

Rational Design and Synthesis of Porous Organic Polymers for Targeted Adsorptive Separation of Model Organic Pollutants

Yixinyu Qin
Chengdu University of Technology
Hongxia Zhu
670553294@qq.com
Chengdu University of Technology
Jian Guo
Chengdu University of Technology
Xuan Gao
Zhejiang University of Science and Technology
Changli Wu
Chengdu University of Technology
Lu Yi
Chengdu University of Technology
Mo Xu
Chengdu University of Technology
Yue Hu
Chengdu University of Technology
Chuankun Liu
Sichuan Academy of Environmental Policy and Planning

Article

Keywords: Porous Organic Polymers (POPs), Bisphenol A (BPA), Adsorption, Cellulose Sponge

Posted Date: November 3rd, 2026

DOI: https://doi.org/10.21203/rs.3.rs-11335800/v1

License: This work is licensed under a Creative Commons Attribution 4.0 International License.
Read Full License

Additional Declarations: No competing interests reported.

Rational Design and Synthesis of Porous Organic Polymers for Targeted Adsorptive Separation of Model Organic Pollutants

Yixinyu Qin[a,b], Hongxia Zhu[a,b,*], Jian Guo[a,b], Xuan Gao[c], Changli Wu[a,b], Lu Yi[a,b], Mo Xu[a,b], Yue Hu[a], Chuankun Liu[d]

[a] State Key Laboratory of Geohazard Prevention and Geoenvironment Protection, Chengdu University of Technology, Chengdu 610059, Sichuan, People's Republic of China

[b] College of Environment and Civil Engineering, Chengdu University of Technology, Chengdu 610059, Sichuan, People's Republic of China

[c] School of Environmental and Natural Resources, Zhejiang University of Science and Technology, Hangzhou 310023, China

[d] Sichuan Academy of Environmental Policy and Planning, Chengdu 610000, China

* Corresponding author: Hongxia Zhu

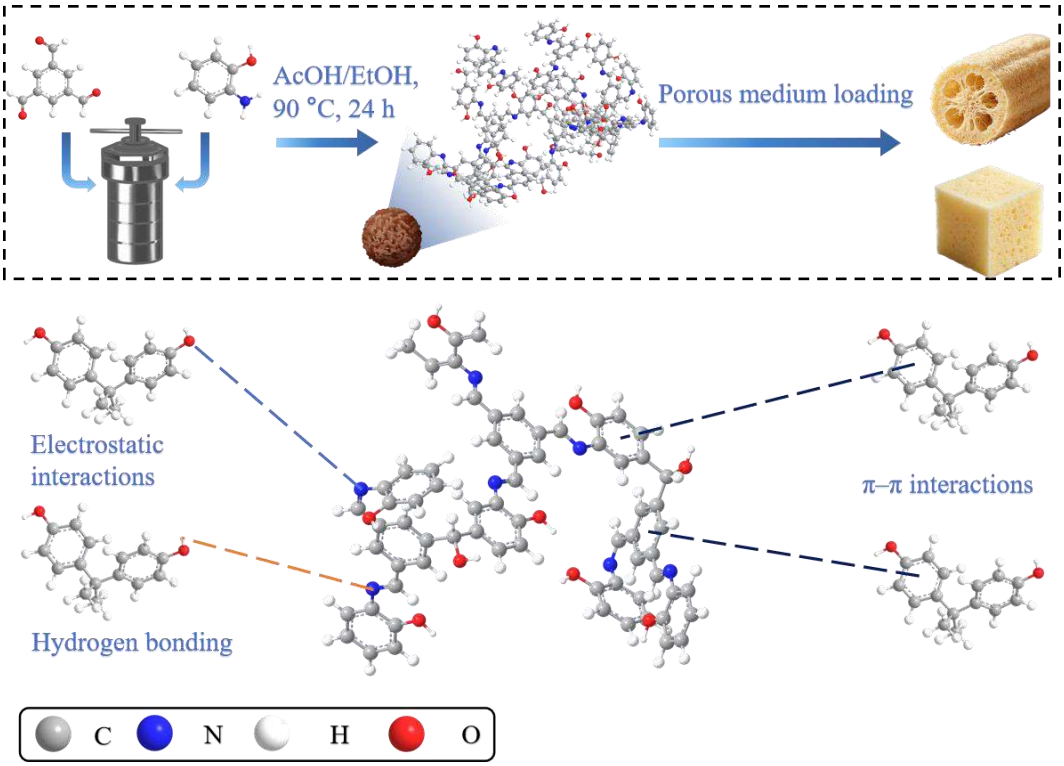
Mobile:13228221513

E-mail: 670553294@qq.com

Abstract: Porous organic polymers (POPs) are promising adsorbents for organic contaminants, but their powdery form hinders recovery and practical deployment. Here, an imine- and aromatic-rich porous organic polymer (TFB/2-AP POP) was synthesized from 1,3,5-triformylbenzene and o-aminophenol by a solvothermal route, with an optimized monomer mass ratio of 4:3. The resulting POP powder showed a BPA adsorption capacity of 215.49 $mg \cdot g^{-1}$. To overcome the handling and recycling limitations of the powder, natural loofah sponge and cellulose sponge were evaluated as macroscopic supports, and an easily recoverable POP@cellulose sponge (POP@CS) monolith was fabricated by ultrasound-assisted loading. POP particles were uniformly distributed on the cellulose sponge skeleton while the interconnected channels were retained. Under neutral conditions, POP@CS achieved an equilibrium adsorption capacity of 171.18 $mg \cdot g^{-1}$ and removed more than 98% of BPA within 6 h at an adsorbent dosage of 0.4 $g \cdot L^{-1}$. The composite maintained strong adsorption over pH 3-11 and reached a maximum capacity of 227.15 $mg \cdot g^{-1}$ at pH 9. Adsorption followed the pseudo-second-order kinetic model and the Freundlich isotherm model. Common coexisting ions caused less than a 25% decrease in BPA removal, and more than 88% of the initial removal performance was retained after five adsorption–desorption cycles. Mechanistic analysis indicated synergistic contributions from π–π electron donor–acceptor interactions, hydrogen bonding, electrostatic attraction, and hierarchical-channel-enhanced mass transfer. This work provides a simple strategy for transforming high-performance POP powders into recyclable monolithic adsorbents for practical removal of phenolic organic pollutants from water.

Keywords: Porous Organic Polymers (POPs); Bisphenol A (BPA); Adsorption; Cellulose Sponge

TOC



1. Introduction

The acceleration of industrialization has led to the frequent detection of new organic pollutants in aquatic environments, including pharmaceuticals, personal care products, perfluorinated compounds, brominated flame retardants, and endocrine disruptors. These substances typically exhibit environmental persistence, bioaccumulation, and endocrine-disrupting toxicity, thereby posing significant threats to ecosystems and human health[1-2].

Bisphenol A (BPA) as a monomer used in epoxy resins and polycarbonate plastic production.They are widely distributed in soil, water, food and Food Packaging[3].BPA's estrogen-mimicking causes a variety of health concerns, including ovarian cancer and breast cancer, as well as reproductive abnormalities, even at extremely low concentrations[4-5].Most bisphenol A (BPA) cannot be efficiently eliminated by traditional wastewater treatment technologies due to its recalcitrance to biodegradation and stable chemical structures[6].

Therefore, there is an urgent need for environmentally efficient, friendly, and cost-effective remediation technologies. In recent years, adsorption technology has been widely studied because of its simple operation and low cost. However, these traditional adsorbent materials such as activated carbon (AC), zeolites, etc. still have certain problems that limit their practical applications, such as low selectivity, low adsorption capacity, poor dispersion stability, and difficulty in regeneration of the adsorbent material[7-8].

In recent years, porous organic polymers (POPs) have emerged as a category of porous materials consisting of organic structural units interconnected by robust covalent bonds, particularly in the domain of organic pollutant adsorption and separation. These materials feature tunable pore sizes, excellent chemical stability, and facile functionalization, positioning them as highly promising candidates for next-generation adsorption applications[9-11]. Particularly, porous organic polymers (POPs) synthesized via dynamic covalent chemistry, such as imine condensation, may display amorphous characteristics; nonetheless, they can still establish porous networks enriched with functional groups. This structural configuration is anticipated to facilitate rapid and high-capacity adsorption of specific pollutants[12].For instance, the maximum adsorption capacity of TFPA-N-β-CD POP material for BPA reported by Zhang et al. was 164.73 $mg \cdot g^{-1}$[13].Zhao et al. synthesized catechol-imine porous organic polymer (CCPOP) materials that exhibited a maximum adsorption capacity of 203.94 $mg \cdot g^{-1}$ for bisphenol A (BPA)[14]. In a separate study, Wei et al. developed a magnetic organic framework, Fe_3O_4@TpND, and employed the Langmuir model to assess its magnetic loading for BPA, achieving a maximum adsorption capacity of 114.97 $mg \cdot g^{-1}$[15].Although Porous Organic Polymers (POPs) have demonstrated efficacy in laboratory-scale adsorption studies, their inherent powder form significantly impedes practical applications. Nanometer- or micrometer-sized POP powders are susceptible to agglomeration, which reduces the effective specific surface area and the availability of active sites. Additionally, these powders are challenging to stabilize in dynamic water flow, leading to potential loss, secondary pollution, and difficulties in recycling. Furthermore, when re-filling the powder form, a substantial pressure drop occurs, posing a risk of inhalation exposure for operators[16]. Consequently, "shaping" POP powders into a molded material with a macroscopic structure, facilitating ease of operation and ensuring stable performance, is a crucial step for transitioning from laboratory settings to real-world water treatment applications. The ideal carrier should exhibit high porosity

to accommodate a substantial quantity of Porous Organic Polymers (POPs), possess adequate mechanical strength to endure hydraulic shock, and maintain environmental compatibility in terms of cost and safety[17]. Among various carriers, cellulose sponge and natural loofah sponge have garnered significant attention due to their widespread availability, low cost, favorable flexibility, biodegradability, and three-dimensional interconnected microporous network structure[18]. The macropores in these materials serve as mass transfer channels, facilitating the diffusion of pollutant molecules into the POP-loaded nanoparticles integrated within their framework. Regarding loading technology, the ultrasonic-assisted method employs micro-jets and shock waves produced by the cavitation effect, effectively disaggregating POP aggregates and enhancing their uniform dispersion within the carrier pores. This method is both efficient and gentle for loading purposes[19].

It is important to highlight that both the modification of inorganic component loading to enhance material functionality and the carrier loading molding aimed at addressing the limitations of powder engineering often result in a reduction of the adsorption capacity of Porous Organic Polymers (POPs) for bisphenol A (BPA). This phenomenon has been substantiated by numerous authoritative studies in the field. Moreover, it represents a critical challenge that must be overcome in the current engineering applications of POPs materials. The core attenuation mechanism can be summarized in three key points. First, loading components tend to clog the channels of porous organic polymers (POPs) and coat the particle surfaces, leading to a decrease in specific surface area and a reduction in mass transfer channels and physical adsorption sites for bisphenol A (BPA)[20]. Second, supported components are likely to interact with active sites, such as imine bonds and hydroxyl groups, on the POPs skeleton, thereby consuming effective chemical adsorption sites that facilitate hydrogen bonding and π-π stacking interactions with BPA[21]. Third, the "dilution effect" of inert carriers diminishes the proportion of effective adsorbed components in the composite material per unit mass, which directly results in a reduced apparent adsorption capacity[22].For example, the magnetic Fe_3O_4-loaded COF developed by Liu et al. exhibited a saturated adsorption capacity for BPA that decreased by 16.7% compared to the original COF, a reduction attributed to the clogging of pores by nanoparticles[20]. Similarly, Wang et al. reported that excessive Cu loading could occupy the active sites of imine bonds in COF, leading to a maximum reduction in BPA adsorption capacity of 34.9%[21]. Consequently, the primary focus of research in this field is to enhance the engineering advantages of POPs materials, such as facilitating recyclability, while maximizing their intrinsic adsorption performance.

This study presents, for the first time, the optimization and synthesis of 1,3,5-triformylbenzene (TFB) and o-aminophenol (2-AP) monomers via a solvothermal method, resulting in an amorphous porous organic polymer (TFB/2-AP POP) characterized by abundant imine bonds and aromatic structures. Additionally, the TFB/2-AP@sponge composite material was fabricated using ultrasonic-assisted technology. The analysis of material properties conducted with an adsorption testing machine elucidated the multiple synergistic adsorption mechanisms of bisphenol A (BPA) by the composite materials, thereby providing a theoretical foundation for their application in complex water environments.

2. Materials and Methods

2.1. Chemical reagents and porous carriers

1,3,5-triformylbenzene (TFB, 96%), o-aminophenol (2-AP, 99%), glacial acetic acid (99.5%), and bisphenol A (BPA, 99%) were obtained from Shanghai Aladdin Biochemical Technology Co. LTD. Anhydrous ethanol was sourced from Sinopharm Chemical

Reagent Co. LTD. All chemical reagents were of analytical grade and utilized without further purification. Ultrapure water (18.2 MΩ·cm) served as the experimental water. The porous carriers consisted of commercially available cellulose sponges, primarily composed of cellulose, and natural loofah sponges, which are dried products. Both types of sponges were cut into small pieces of approximately 1 cm^3, ultrasonically cleaned with anhydrous ethanol and ultrapure water, and dried at 60℃ until a constant weight was achieved for subsequent use. Following a comparison of adsorption performance, the cellulose sponge was identified as the core loading carrier.

2.2. Solvothermal Synthesis and Optimization of TFB/2-AP POP

TFB/2-AP POP was synthesized using a solvothermal method. The specific synthesis steps are as follows: Different masses of TFB (0.1, 0.15, 0.2, 0.4 g) were dissolved in 25 mL of anhydrous ethanol, along with a fixed mass of 2-AP (0.15 g). The mixture was then combined, and 0.5 mL of glacial acetic acid was added as a catalyst. The resulting solution was transferred to a 100 mL stainless steel reactor lined with polytetrafluoroethylene, which was subsequently sealed and placed in an oil bath at 90°C for a reaction period of 24 hours. Upon completion of the reaction, the mixture was allowed to cool naturally to room temperature. The resulting yellow precipitate was collected by centrifugation (8000 rpm, 10 min) and washed successively with anhydrous ethanol and ultrapure water to eliminate unreacted monomers and catalysts. The final product was dried to a constant weight in a vacuum oven at 60°C to yield POP powders with varying monomer mass ratios (TFB:2-AP = 2:3, 1:1, 4:3, 8:3), designated as TFB/2-AP-X (where X denotes the mass of TFB). The performance of the products with different monomer ratios was assessed through pre-adsorption experiments conducted under the following conditions: 50 $mg \cdot L^{-1}$ BPA, 50 mL solution volume, 10 mg adsorbent dosage, and an adsorption duration of 6 hours. The optimal synthesis ratio of 4:3 was identified for subsequent studies.

2.3. Ultrasonic-assisted preparation of formed composite materials

The optimal proportion of TFB/2-AP POP was loaded onto pre-treated cellulose sponge and natural loofah sponge using an ultrasonic-assisted impregnation method. Initially, 0.08 g of TFB/2-AP POP powder was dispersed in 20 mL of anhydrous ethanol and subjected to ultrasonic treatment (200 W, 40 kHz) for 30 minutes to create a uniform suspension. Subsequently, 0.32 g of the pre-treated sponge blocks and 0.32 g of the pre-treated natural loofah sponge were immersed in this suspension and treated for an additional hour under the same ultrasonic conditions. During this process, ultrasonic cavitation facilitated the penetration and uniform adhesion of POP particles within the three-dimensional network of the sponge and the grid structure of the natural loofah sponge. Upon completion of the loading process, the composite material was removed and dried at 60°C until a constant weight was achieved, resulting in the final products designated as TFB/2-AP@ sponge and TFB/2-AP@ natural loofah sponge.

2.4. Material Characterization techniques

The microscopic morphology of the POP powder and composite materials was examined using field emission scanning electron microscopy (FE-SEM, Hitachi SU8010). Prior to testing, the samples were gold-sprayed to enhance conductivity. The material's crystallinity was assessed with an X-ray polycrystalline diffractometer (XRD, Malvern Panalytical X 'pert3 Powder, Cu Kα radiation). Specific surface area and pore size distribution were determined through nitrogen adsorption and desorption tests at 77 K, employing an automatic specific surface area and porosity analyzer (ASAP 2460). These parameters were calculated using the BET and BJH models, respectively[23]. The elemental composition and chemical state of the material surface were analyzed via

X-ray photoelectron spectroscopy (XPS, Thermo Scientific K-alpha, Al Kα ray source)[24]. The binding energy was calibrated to the 1s peak of adventitious carbon (C) at 284.8 eV. Functional group information was obtained using the KBr pellet method within the range of 4000-400 cm^{-1}, employing a Fourier transform infrared spectrometer (FT-IR, Thermo Nicolet iS50).

2.5. Adsorption Performance Tests

All adsorption experiments were performed in a shaker maintained at a constant temperature of (25 ± 1°C) and a rotational speed of 150 rpm. The concentration of BPA was measured using a UV-Vis spectrophotometer (Shimadzu UV-2600) at a maximum absorption wavelength of 276 nm.

In the adsorption kinetics experiment, 8.0 mg of adsorbent (either pure POP or POP@sponge) was added to 50 mL of BPA solution with an initial concentration of 50 $mg \cdot L^{-1}$, ensuring that the solution remained neutral. Samples were collected at predetermined time intervals (0, 1, 2, 4, 6, 12, 24, and 48 hours), and the remaining concentration was measured following filtration. The data were analyzed using quasi-first-order and pseudo-second-order dynamic models[25].

Adsorption isotherm experiments involved the addition of 8.0 mg of adsorbent to 50 mL of BPA solutions with varying initial concentrations of 10, 20, 30, 40, and 50 $mg \cdot L^{-1}$. The solutions were maintained under neutral conditions and allowed to adsorb for 24 hours to achieve equilibrium. The resulting equilibrium data were analyzed using the Langmuir and Freundlich isotherm models[26].

In the pH value influence experiment, the initial pH of a 50 $mg \cdot L^{-1}$ BPA solution was adjusted to 3.0, 5.0, 7.0, 9.0, and 11.0 with the addition of 0.1 M HCl or NaOH solution. Following this adjustment, 8.0 mg of adsorbent was introduced, and the equilibrium concentration and final pH were measured after 6 hours of adsorption.

In the coexistence ion interference experiment, 0.01 M solutions of NaCl, $NaNO_3$, Na_2SO_4, or NaH_2PO_4 were individually added to a 50 $mg \cdot L^{-1}$ BPA solution to investigate the effects of common inorganic salt ions on the BPA adsorption performance of POP@sponge.

Adsorbent cycle regeneration experiment: Upon reaching adsorption saturation, the POP@sponge composite material underwent ultrasonic washing with anhydrous ethanol for 30 minutes to facilitate desorption, followed by drying at 60°C in preparation for the subsequent adsorption cycle. This procedure was repeated five times to assess the material's regenerative performance.

3. Results and Discussion

3.1 Synthesis Reaction Mechanism of TFB/2-AP Porous Organic Polymer

The construction of the POPs framework in this study is predicated on the fundamental principle of acid-catalyzed aldehyde-amine condensation, known as the Schiff base reaction. This reaction occurs spontaneously in a solvothermal system of anhydrous ethanol at 90 °C, facilitated by glacial acetic acid. The aldehyde group of 1,3,5-triformylbenzene (TFB) undergoes dehydration condensation with the primary amino group of o-aminophenol (2-AP), resulting in the formation of imine bonds characterized by conjugated stability (-C=N-). This pathway represents the most traditional synthetic route for imine-type porous

organic polymers[3]. The Schiff base reaction can be delineated into two principal steps: nucleophilic addition and dehydration elimination. The entire process can be efficiently executed under the experimental conditions established in this study.

Nucleophilic addition results in the formation of a tetrahedral intermediate. The primary amino nitrogen atom in the o-aminophenol (2-AP) molecule possesses a pair of unshared electron pairs, rendering it nucleophilic. In the aldehyde group of 1,3,5-triformylbenzene (TFB), the electronegativity of the oxygen atom exceeds that of the carbon atom. This induction effect diminishes the electron cloud density around the carbonyl carbon atom, enhancing its electrophilicity. During the reaction, the primary amino nitrogen atom of 2-AP engages in a nucleophilic addition with the carbonyl carbon atom of TFB, leading to the formation of a tetrahedral transition state. Following intramolecular proton transfer, a hemiaminal intermediate is produced.

Dehydration elimination leads to the formation of conjugated imine bonds. In the acidic environment provided by glacial acetic acid, the hydroxyl group (-OH) of the hemiaminal intermediate is protonated to form a good leaving group ($-H_2O^+$), which is eliminated as a water molecule. Simultaneously, the remaining hydrogen on the primary amino group is released as H^+, resulting in the formation of a highly conjugated imine bond (-C=N-), thus completing the condensation reaction.

The single-step aldehyde-amine condensation can facilitate only the intermolecular connection between TFB and 2-AP, failing to establish a three-dimensional cross-linked network. The successful construction of the three-dimensional framework of the indefinite polymer in this study relies on the concurrent occurrence of the phenolic condensation reaction, which is catalyzed by acid. The phenolic hydroxyl group of 2-AP activates the active hydrogen at the o/para position of the benzene ring, rendering it a multifunctional reactive monomer that undergoes cross-linking condensation with the aldehyde group of TFB. This process ensures that the system satisfies the critical condition of "average functionality $f > 2$" as outlined in Carothers' gel point theory, ultimately resulting in the formation of an infinitely extended three-dimensional covalent cross-linked network[27-28].

The two monomers in this system are both multifunctional reactive monomers that can form a three-dimensional cross-linked network under acid-catalyzed conditions. TFB is characterized by a single molecule containing three equivalent aldehyde groups, allowing it to participate in Schiff's base condensation and phenolic aldehyde condensation reactions, thus classifying it as an A3 type trifunctional monomer. In contrast, 2-AP possesses one primary amino group capable of undergoing a Schiff base reaction. Additionally, the strong electron-donating effect of the phenolic hydroxyl group significantly activates the C-H bonds at the 4 (para-position relative to the phenolic hydroxyl group) and 6 (ortho-position relative to the phenolic hydroxyl group and para-position relative to the amino group) positions on the benzene ring. Under acid catalysis, these activated bonds can engage in electrophilic addition-condensation reactions with aldehyde groups. Consequently, 2-AP serves as a multifunctional cross-linked monomer with a minimum of three reaction sites, facilitating cross-linking.

The complete construction of a three-dimensional cross-linked network can be delineated into three distinct steps. First, the formation of basic branching units occurs when a trifunctional TFB molecule reacts with multiple 2-AP molecules. In this process, some aldehyde groups undergo Schiff base condensation with amino groups, while others engage in phenolic condensation with the phenolic hydroxyl groups at the ortho- and para-positions of 2-AP. This reaction results in branched units that feature TFB as the core and 2-AP as the side chains, each containing numerous active sites capable of further reactions.

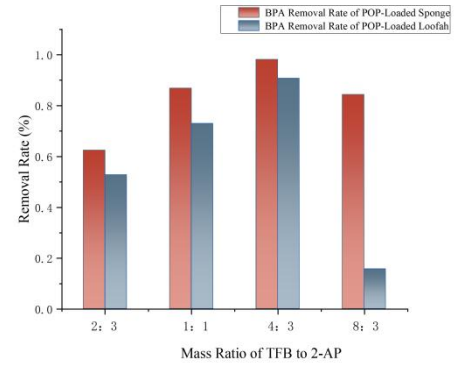
Second, intermolecular crosslinking extension takes place, wherein the 2-AP molecule simultaneously connects two or more distinct TFB branching units through a combination of amino-Schiff base condensation and phenol-hydroxyl ortho-para-phenolic condensation. This process establishes the core bridge points of the cross-linking network. Finally, the three aldehyde groups of TFB extend into three-dimensional space, facilitating the connection of different 2-AP molecules and achieving covalent cross-linking and spatial extension among the branching units.

Gelation and Network Formation: As the reaction progresses, the degree of crosslinking within the system steadily increases. Upon reaching the critical threshold defined by Carothers' gel point theory, the system establishes an infinitely extended three-dimensional covalent crosslinking network. This transition results in the precipitation of the material from the solution, yielding an insoluble and infusible polymer solid, specifically the TFB/2-AP POP synthesized in this study.

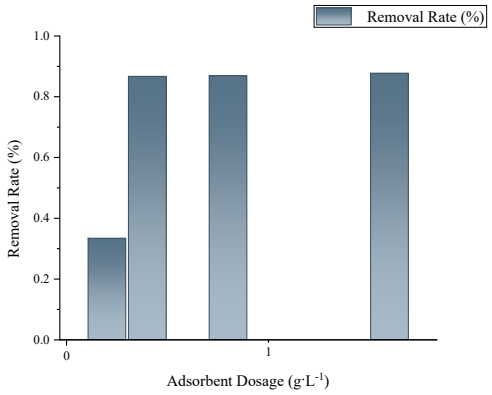
3.2 Material Optimization: Monomer Ratio and Carrier Selection

The ratio of synthetic monomers significantly affects the structure and adsorption performance of porous organic polymers (POP). As illustrated in Figure 1 a, a mass ratio of TFB to 2-AP of 4:3 results in the highest removal rate of bisphenol A (BPA) (98.18%) for the TFB/2-AP POP loaded onto cellulose sponge. This optimized ratio enhances the density of imine bonds (-C=N-) while reducing the clogging or competitive adsorption of unreacted monomers within the pores. Under this feeding ratio, the total amount of aldehyde groups in TFB and the ratio of potential reaction sites, comprising amino groups and phenolic hydroxyl active hydrogen in 2-AP, are maintained within an optimal equilibrium range. This balance not only ensures a sufficient degree of crosslinking to form a stable polymer framework but also mitigates issues related to poor product solubility and structural instability that can arise from inadequate crosslinking. Furthermore, it prevents excessive crosslinking and the embedding of active sites due to an overabundance of TFB (in a ratio of 8:3), while maximizing the retention of adsorption active sites, such as imine bonds and phenolic hydroxyl groups, thereby achieving optimal BPA adsorption performance. Additionally, it avoids the potential for excessive 2-AP (in a ratio of 2:3) to result in an overabundance of residual free amino groups, which could occupy the pores and increase the hydrophilicity of the material.

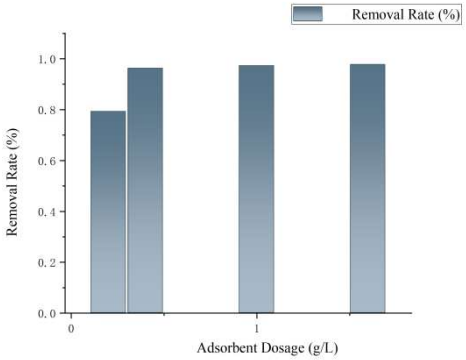
From the perspective of carrier characteristics, natural loofah sponge, a natural biomass material, is directly extracted from agricultural waste without the need for complex processing, thereby facilitating resource reuse. This material offers the dual benefits of low cost and environmental sustainability, aligning with the principles of sustainable development. However, regarding adsorption performance, the BPA removal rate of natural loofah sponge loaded with COF was consistently lower than that of cellulose sponge, irrespective of the proportion of monomers (Figure 1 a). Consequently, all subsequent studies focused on POP with TFB:2-AP in a ratio of 4:3 and its composite materials supported by cellulose sponge.



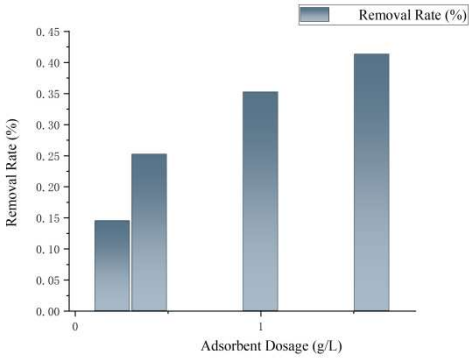
(a) BPA Removal Efficiency of POPs Supported on Two Different Carriers under Different Monomer Mass Ratios



(b) BPA Removal Efficiency of TFB/2-APPOP



(c) BPA Removal Efficiency of the POP-Loaded Sponge



(d) BPA Removal Efficiency of the Cellulose Sponge

Figure 1. (a) The removal rate of BPA by POP loaded on two carriers at varying monomer mass ratios; (b-d) The effect of different adsorbent dosages on the removal rate and equilibrium adsorption capacity of BPA.

The dosage of the adsorbent is a critical parameter influencing the economic efficiency of practical applications. As illustrated in Figure 1 b, the total removal rate for pure POP powder increases with dosage; however, the adsorption capacity per unit mass (q_e) declines sharply. This decline is attributed to the reduced utilization of active sites resulting from particle aggregation. In contrast, the POP@sponge composite achieved a removal rate exceeding 96% at a relatively low dosage of 20 mg, corresponding to only 4 mg of POP (Figure 1 c), while maintaining a high q_e value. The adsorption contribution of the pure sponge is minimal (Figure 1 d). This finding indicates that the sponge carrier significantly enhances the utilization efficiency of POP by preventing aggregation and exposing more active sites.

3.3 Characterization of Structure and Properties of Composite Materials

SEM images (Figure 2a-c) reveal that the synthesized TFB/2-AP POP predominantly consists of agglomerated sub-micron-sized spherical particles, exhibiting a rough surface and a characteristic amorphous polymer morphology. A comparison of the cellulose sponge before (Figure 2d) and after loading (Figure 2e-f) demonstrates that POP particles are uniformly adhered to the smooth skeleton surface of the cellulose sponge, without completely obstructing the original macroscopic channels. This configuration

establishes a multi-level pore system comprising "macropores (sponge) - mesoporous/micropores (POP)," which facilitates the rapid movement of water and provides pathways for the diffusion of BPA molecules to the active sites of POP.

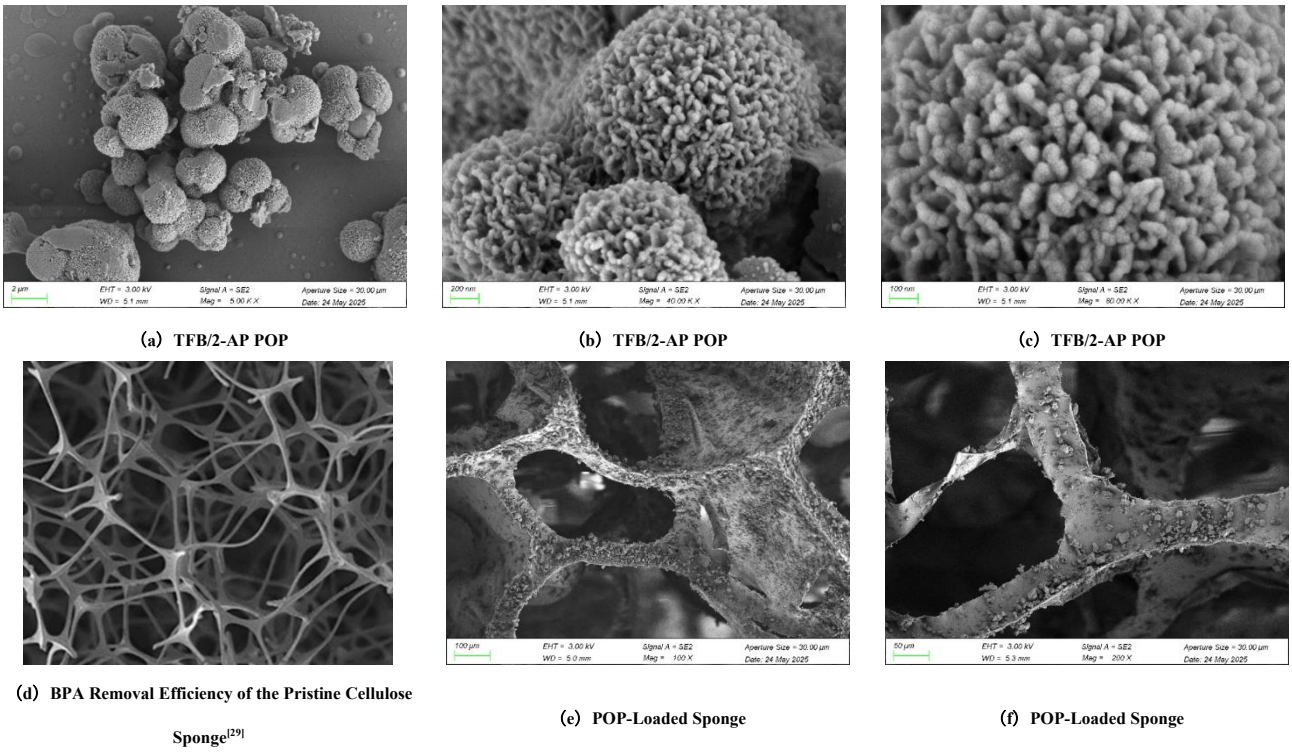


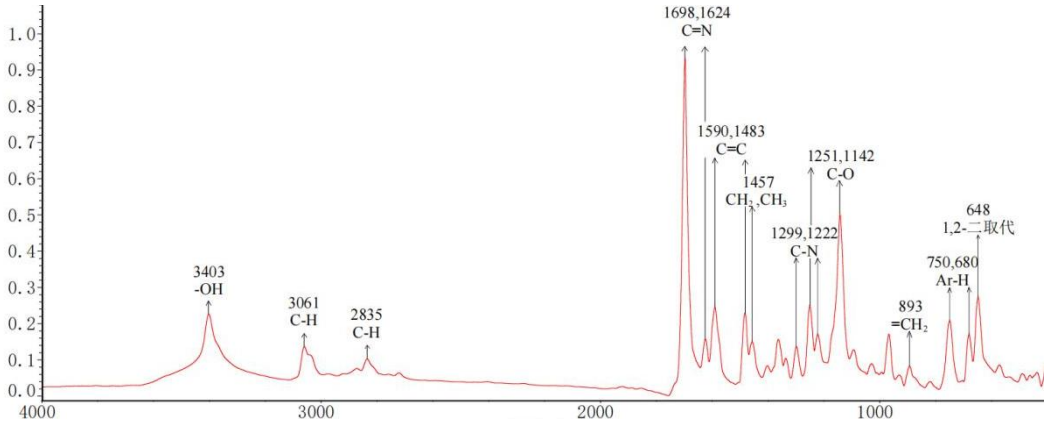
Figure 2. (a-c) Scanning electron microscopy (SEM) images of TFB/2-AP powder; (d) SEM image of the unloaded fiber sponge; (e-f) SEM images of the loaded sponge.

The XRD pattern (Figure S1) reveals the absence of sharp diffraction peaks in the low-angle region, thereby confirming the material's amorphous structure. This observation aligns with the simultaneous occurrence of Schiff base condensation and phenolic condensation, which leads to the formation of a randomly cross-linked polymer network. The N_2 adsorption and desorption test indicates that the BET specific surface area of the material is merely 0.19 $m^2 \cdot g^{-1}$, accompanied by a notably low total pore volume. This finding is consistent with the structural characteristics of randomly cross-linked amorphous polymers bearing phenolic hydroxyl groups, although the specific surface area of this polymeric organic framework (POP) is significantly lower than that of typical porous framework materials, such as COFs and MOFs. Nevertheless, it demonstrates an impressive adsorption capacity (171-227 $mg \cdot g^{-1}$) and rapid adsorption kinetics for BPA. This behavior suggests that the material's adsorption performance primarily arises from the multiple synergistic effects—such as π - π electron donor-acceptor interactions, hydrogen bonding, and electrostatic attraction—conferred by the densely distributed aromatic rings, imine bonds, and amino functional groups within its structure, rather than depending on the physical pore architecture.

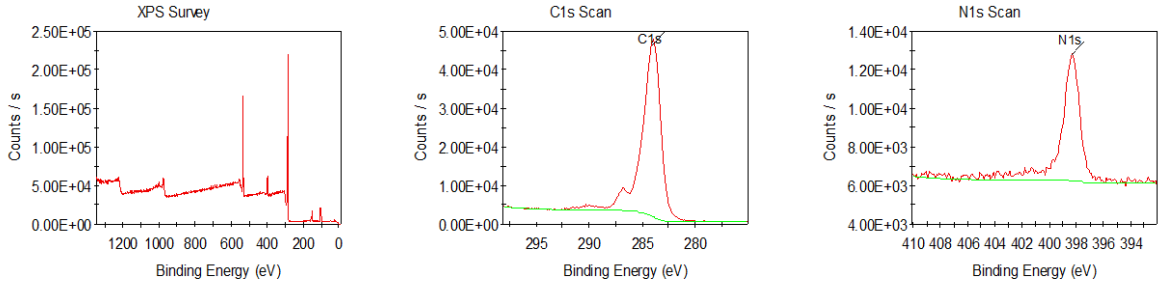
The full spectrum of X-ray photoelectron spectroscopy (XPS) (Figure 3b) indicates that the material predominantly consists of carbon (C), nitrogen (N), and oxygen (O) elements. The high-resolution C 1s spectrum (Figure 3c) can be deconvoluted into three distinct peaks: 284.8 eV (C-C/C-H), 286.2 eV (C=N/C-N), and 288.5 eV (C=O). The presence of the C=N/C-N peak is corroborated by the Fourier-transform infrared (FT-IR) results. In the high-resolution N 1s spectrum, the characteristic peak at 399.5 eV is attributed to the nitrogen atom of the imine bond (-C=N-), thereby confirming the structural integrity of the Schiff base product. The peak at 401.2 eV is associated with protonated imine nitrogen (-CH=NH^+-) or a minor fraction of residual protonated primary amino groups, which may impart a positive charge to the material's surface across a broad pH range, thus

facilitating electrostatic adsorption[24]. This observation aligns with the characteristics typical of an acidic synthetic environment. The peak at 284.8 eV in the C 1s high-resolution spectrum corresponds to the C-C/C-H structure of the aromatic ring, while the fitted peak at 286.2 eV is linked to the C=N structure of the imine bond. The peak at 288.5 eV corresponds to the C=O structure of the unreacted aldehyde group, consistent with the proposed reaction mechanism.

FT-IR spectra (Figure 3a) provide evidence for the formation of imine bonds. The strong characteristic absorption peaks at 1624 cm^{-1} and 1698 cm^{-1}, which correspond to the stretching vibration of the imine bond (-C=N-), confirm the occurrence of the core Schiff base reaction. This finding aligns with the reported infrared characteristic peaks of imine-type polymers[3]. The broad peak at 3403 cm^{-1} corresponds to the O-H stretching vibration, indicating that the phenolic hydroxyl group in the 2-AP molecule was partially retained during the polymerization process and did not fully participate in the phenolic condensation reaction. This retention provides a site for hydrogen bond interactions in subsequent BPA adsorption, forming a closed loop with the adsorption mechanism. The characteristic peak at 1251 cm^{-1} corresponds to the C-O stretching vibration of the phenolic hydroxyl group on the aromatic ring, further confirming the retention of the phenolic hydroxyl group. Additionally, the aromatic C-H vibration at 3061 cm^{-1} and the aromatic ring skeleton vibration at 1590 cm^{-1} confirm that the aromatic structure in the polymer skeleton was completely retained, thereby providing a structural basis for the π-π interaction in BPA adsorption.



(a) Fourier Transform Infrared (FTIR) Spectrum of TFB/2-AP POP



(b) X-ray Photoelectron Spectroscopy (XPS) Survey Spectrum

(c) C1s High-Resolution Spectrum

(d) N1s High-Resolution Spectrum

Figure 3. (a) FT-IR spectrum of TFB/2-AP POP; (b-d) complete XPS spectrum and high-resolution C 1s and N 1s spectra.

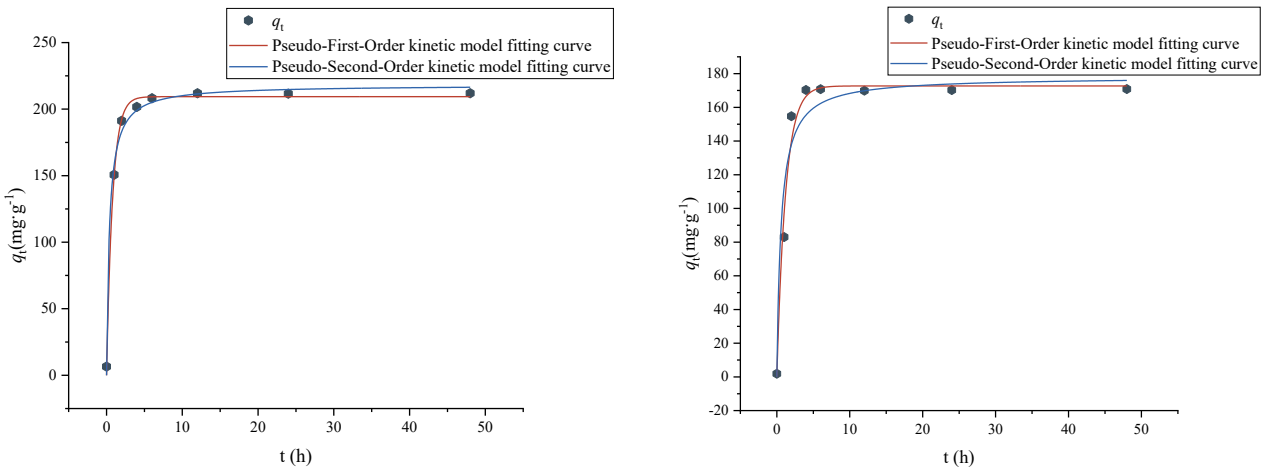
3.4. Adsorption Performance Evaluation

3.4.1. Adsorption Kinetics

The adsorption kinetics of bisphenol A onto pure POP materials and their sponge-supported composite counterparts are illustrated in Figure 4. The adsorption processes for both types of materials display the characteristic pattern of "rapid adsorption followed by slow equilibrium"; however, notable differences exist in their adsorption rates and equilibrium capacities. Pure POP materials demonstrate an exceptionally high adsorption rate during the initial phase (0 to 2 h), with the adsorption capacity increasing swiftly from 0 to approximately 200 $mg \cdot g^{-1}$. They reach adsorption equilibrium around 5 h, with an equilibrium capacity of approximately 215.49 $mg \cdot g^{-1}$. This observation suggests that the surface of pure POP possesses a high density of accessible adsorption sites, facilitating the rapid diffusion of bisphenol A molecules through the liquid film and their binding to active sites with minimal mass transfer resistance. The pseudo-second-order kinetic model aligns closely with the experimental data, as evidenced by the high correlation between the curve and the experimental points. This further substantiates that the adsorption process is primarily governed by chemical adsorption, wherein bisphenol A interacts with the surface functional groups of POP to establish stable bindings through electron sharing or transfer[25].

In contrast, the initial adsorption rate of the POP-supported sponge composite material exhibited a slight decrease. The adsorption capacity increased to approximately 170 $mg \cdot g^{-1}$ within the first 2 hours and reached adsorption equilibrium around 10 hours, at which point the equilibrium adsorption capacity declined to approximately 171.18 $mg \cdot g^{-1}$. The prolonged equilibrium time and the reduction in adsorption capacity primarily result from the introduction of sponge carriers. Specifically, the porous structure of the sponge lengthens the diffusion path for bisphenol A, causing some encapsulated POP active sites to take longer to become occupied. Additionally, the sponge itself lacks adsorption capacity, effectively diluting the concentration of available adsorption sites within the system and thereby reducing the adsorption capacity per unit mass of the composite material. Nevertheless, the pseudo-second-order dynamics model continues to fit the data post-loading, indicating that the sponge functions solely as a physical support and does not alter the fundamental mechanism of chemical adsorption between POP and bisphenol A.

In conclusion, pure POP materials demonstrate superior adsorption kinetics. The fitted kinetic parameters are summarized in Table 1. While composite materials supported by sponges exhibit a slight reduction in both capacity and rate, they markedly improve the operability and practical applicability of the materials. This enhancement offers a more viable option for future engineering applications in water treatment scenarios.



(a) Pseudo-First-Order and Pseudo-Second-Order Kinetic Model Fitting of TFB/2-AP POP

(b) Pseudo-First-Order and Pseudo-Second-Order Kinetic Model Fitting of the POP-Loaded Sponge

Figure 4. Kinetics curve of BPA adsorption by POP@sponge; (b) Fitting diagram for the pseudo-second-order dynamic model.

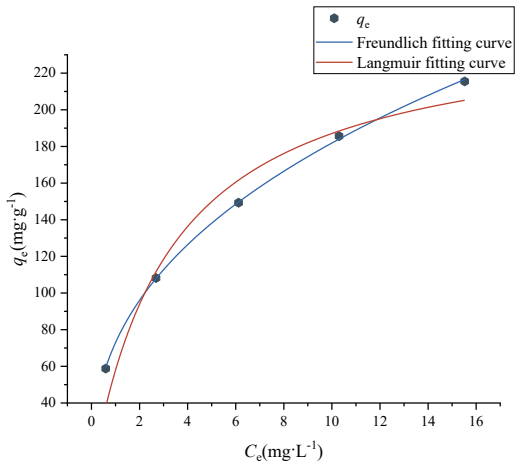
Table 1. Kinetic model fitting parameters for BPA adsorption by TFB/2-AP POP and POP-loaded sponge.

Pollutant	Adsorbent	Pseudo-first-order			Pseudo-second-order		
		k_1	q_e	R^2	k_2	q_e	R^2
BPA	TFB/2-AP	1.509	208.427	0.349	0.0198	212.765	0.999
	POP-Loaded Sponge	0.901	182.956	0.258	0.0251	172.117	0.999

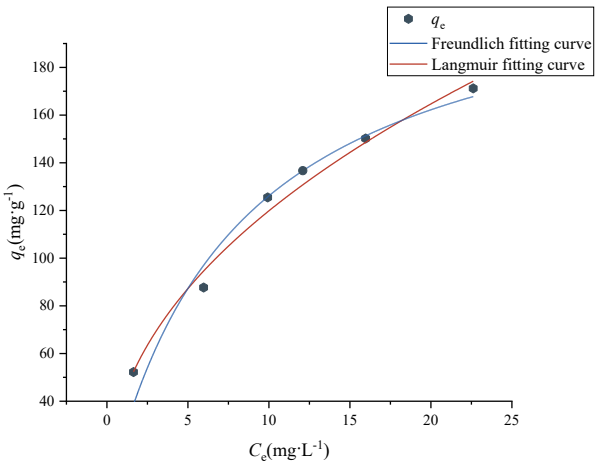
3.4.2 Adsorption isotherm

The adsorption isotherms of pure POP and POP-supported sponges at varying initial concentrations are depicted in Figure 5. The adsorption capacities of both pure POP and POP@sponge for BPA increase with the equilibrium concentration, exhibiting a rapid rise in the low concentration range followed by a gradual plateau in the high concentration range. For pure POP materials (Figure 5a), fitting with the Langmuir and Freundlich models revealed that the Freundlich model demonstrated a superior goodness of fit (R^2=0.992) compared to the Langmuir model (R^2=0.985). This finding suggests that adsorption occurs on heterogeneous surfaces and exhibits multilayer adsorption characteristics[26]. Additionally, the Freundlich constant $1/n$=0.421 (1) indicates that this adsorption process is readily facilitated.

For the POP@sponge composite materials (Figure 5b), the Freundlich model (R^2=0.988) exhibits a marginally superior fit compared to the Langmuir model (R^2=0.986). This finding indicates that, following the loading of the sponge, adsorption continues to occur on the heterogeneous surface, preserving the characteristics of multilayer adsorption. The Freundlich constant $1/n$=0.465 (1) suggests that the adsorption process is readily facilitated. The isotherm behavior of both materials, along with the model fitting results, demonstrates that the loaded sponge does not alter the adsorption characteristics of POP on BPA. Instead, only the dilution effect of the sponge carrier slightly diminishes the adsorption capacity. The adsorption-isotherm fitting parameters are summarized in Table 2.



(a) Adsorption Isotherm Model Fitting of TFB/2-AP POP



(b) Adsorption Isotherm Model Fitting of the POP-Loaded Sponge

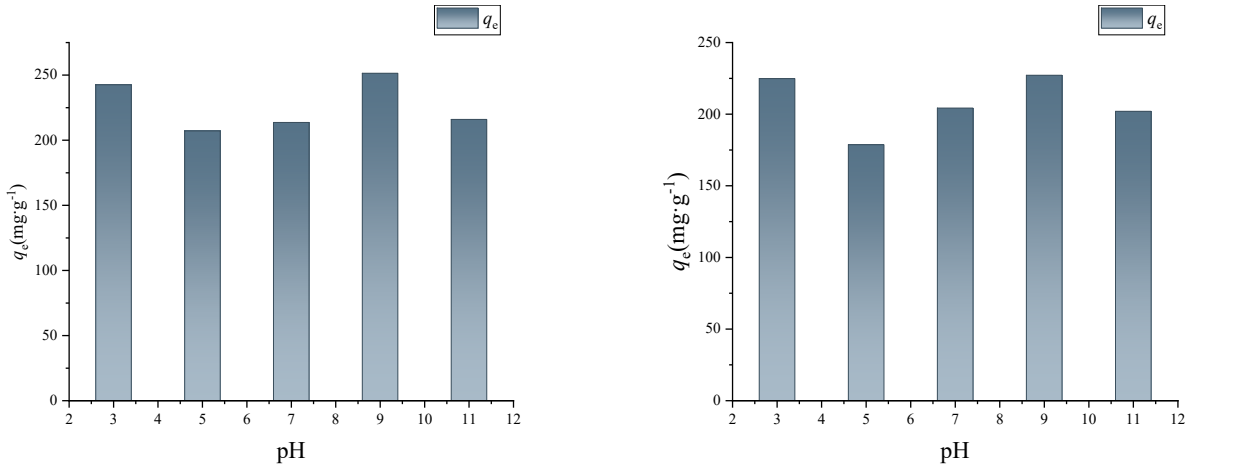
Figure 5. (a) (b) Fitting of the adsorption isotherm model of pure POP/ POP@sponge for BPA

Table 2. Fitting of TFB/2-AP and loaded sponge adsorption isotherm models

Pollutant	Adsorbent	Langmuir Model Fitting			Freundlich Model Fitting		
		R_L	q_m	R^2	k_F	$1/n$	R^2
BPA	TFB/2-AP	0.338	248.37	0.989	72.457	0.421	0.992
	POP-Loaded Sponge	0.058	192.61	0.986	40.894	0.465	0.988

3.4.3Analysis of the influence Mechanism of pH on Adsorption Performance

The pH of the solution significantly influences adsorption performance by affecting the surface charge of the adsorbent and the chemical form of BPA (pKa ≈ 9.6). As illustrated in Figure 6, POP@sponge exhibits a high adsorption capacity across a broad pH range of 3 to 11. In acidic to neutral conditions (pH 3-7), BPA predominantly exists as a neutral molecule, with adsorption primarily facilitated by hydrogen bonds and π-π interactions. At pH 9, which is close to the pKa of BPA, the adsorption capacity peaks at 227.15 $mg \cdot g^{-1}$. This increase may be attributed to the deprotonation of some BPA molecules, resulting in a negative charge that enhances electrostatic attraction with the protonated amino groups ($-NH_3^+$) on the surface of POP, thereby creating a synergistic effect with hydrogen bonds and π-π interactions. Under strongly alkaline conditions (pH 11), BPA is fully deprotonated, leading to an increase in the negative charge on the surface of POP. This change results in heightened electrostatic repulsion and a reduction in adsorption capacity. Nevertheless, the adsorption capacity remains substantial, demonstrating the material's commendable environmental adaptability.



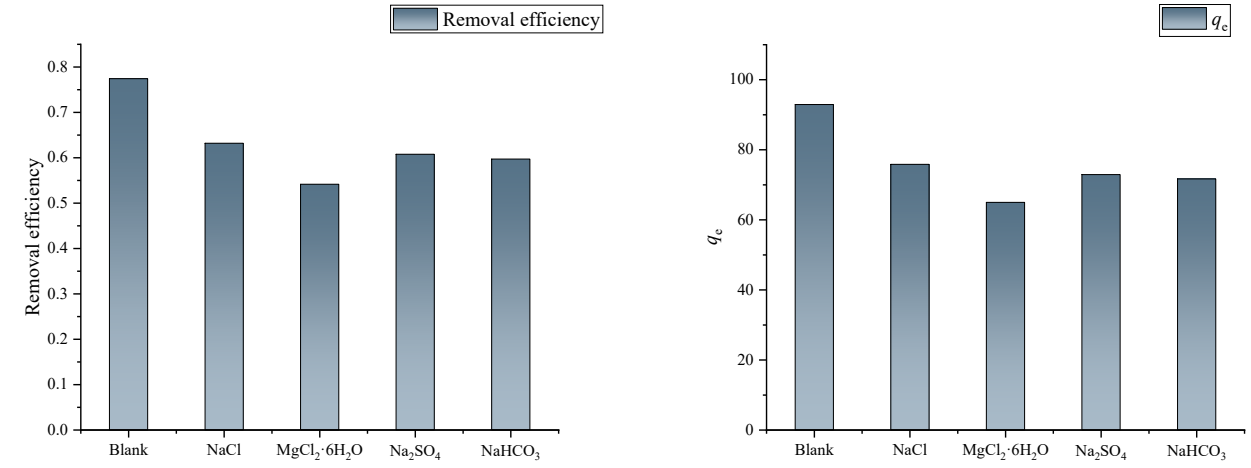
(a) BPA Removal Efficiency of TFB/2-AP POP under Different pH Values

(b) BPA Removal Efficiency of the POP-Loaded Sponge under Different pH Values

Figure 6. The influence of the initial pH of the solution on the BPA adsorption performance of POP/ POP@sponge.

3.4.4. Coexisting ion interference and Cycling stability

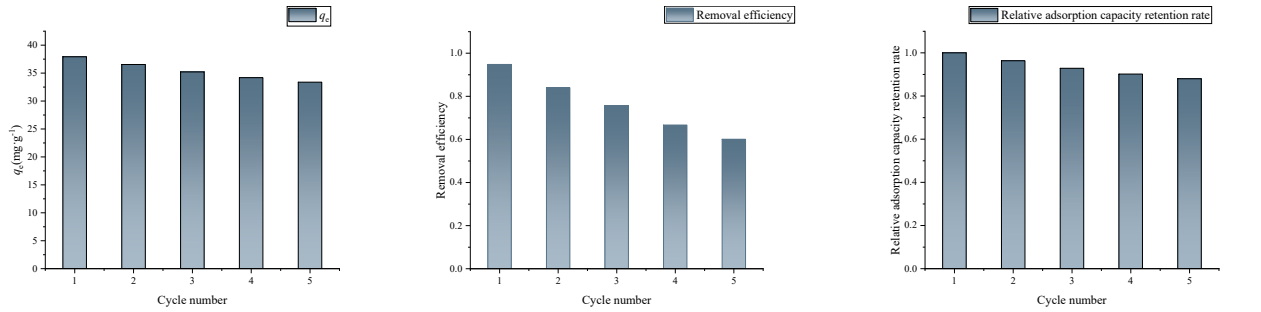
Coexisting ion interference experiments showed that common inorganic ions in water (Cl^-, SO_4^{2-}, HCO_3^-, Mg^{2+}) had a limited inhibitory effect on BPA adsorption by POP@sponge, with the removal rate decreasing by less than 25%. This indicates that the material has good anti-interference ability in complex water bodies. Furthermore, after five adsorption-desorption cycles, the BPA removal rate of POP@sponge remained above 88% of the initial value, confirming that ultrasonic washing with anhydrous ethanol is an effective regeneration method and the material has good reusability. The coexisting-ion results are shown in Figure 7, and the adsorption–desorption cycling results are shown in Figure 8, respectively.



(a) BPA Removal Efficiency of the POP-Loaded Sponge under Different Coexisting Ion Systems

(b) Equilibrium Adsorption Capacity of the POP-Loaded Sponge for BPA under Different Coexisting Ion Systems

Figure 7. The influence of coexisting ions on the adsorption performance of BPA by TFB/2-AP POP



(a) Equilibrium Adsorption Capacity of the POP-Loaded Sponge for BPA under Different Cycle Numbers

(b) BPA Removal Efficiency of the POP-Loaded Sponge under Different Cycle Numbers

(c) Relative Adsorption Capacity Retention Rate of the POP-Loaded Sponge under Different Cycle Numbers

Figure 8. Cyclic adsorption and regeneration performance of TFB/2-AP@ sponge composite material

3.4.5. Comparison of BPA Adsorption Performance

To further assess the practical application potential of the TFB/2-AP@ sponge composite material developed in this study, its adsorption performance for BPA was compared with that of similar cellulose-based supported adsorption materials, POPs/COFs-based powder materials, and conventional mainstream adsorbents, as illustrated in Figure 9.The comparison results indicate that the neutral condition saturated adsorption capacity of the composite material developed in this study for BPA reaches 171.18 $mg \cdot g^{-1}$. This capacity is significantly higher than that of previously reported cellulose sponge-supported COFs materials (112.0-138.5 $mg \cdot g^{-1}$)[30-31], β-cyclodextrin-modified COFs (108.6 $mg \cdot g^{-1}$)[34], MOFs-derived carbon materials (124.7 $mg \cdot g^{-1}$)[35], and modified biomass activated carbon (98.6 $mg \cdot g^{-1}$)[36]. Under weakly alkaline conditions at pH=9, the adsorption capacity further increases to 227.15 $mg \cdot g^{-1}$, demonstrating even greater advantages. Regarding adsorption kinetics, this material requires a low adsorbent dosage of 0.4 $g \cdot L^{-1}$ to achieve a removal rate of 98.18% for 50 $mg \cdot L^{-1}$ BPA within 6 hours. This performance significantly surpasses that of magnetic COP materials (93%)[33] and hypercross-linked POPs materials (90%)[32] under identical experimental conditions, with a shorter equilibrium time and a notable advantage in adsorption rate.

Notably, this study successfully converted nanoscale POP powder into a macroscopic monolithic material, which is easy to handle and can be directly salvaged and recycled through a cellulose sponge loading strategy, albeit with a slight reduction in adsorption capacity. This advancement effectively addresses the engineering challenges associated with powder materials, including agglomeration, high column pressure, and material loss. Furthermore, the material exhibits stable adsorption performance across a broad pH range of 3 to 11. After five adsorption-desorption cycles, the removal rate of BPA remains above 88%, demonstrating cycle stability that surpasses that of most similar materials reported in the literature[30-31,35-36]. Consequently, this material shows enhanced applicability for the treatment of complex water bodies, compared to most previously reported pure powder POPs/COFs materials[32,34,37].

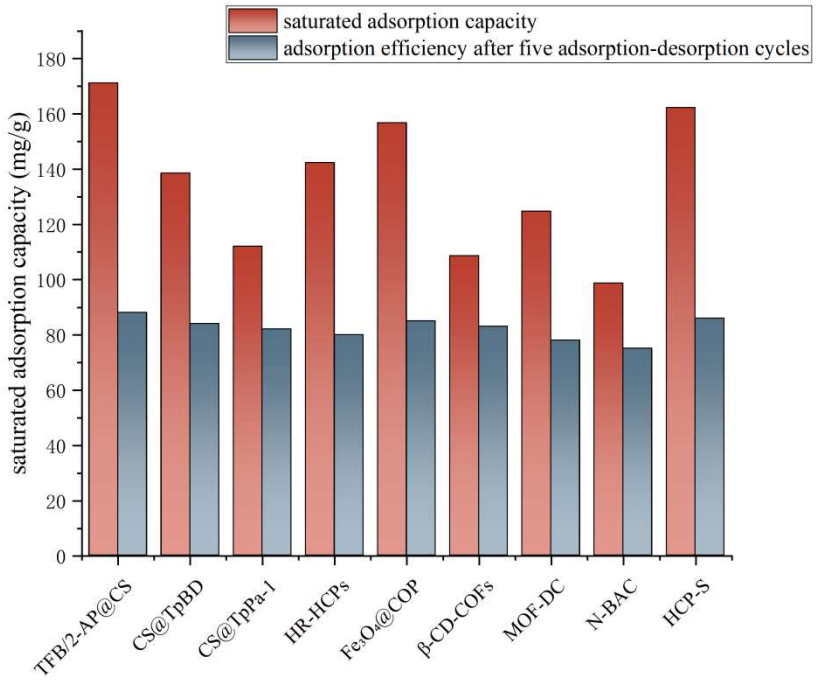


Figure 9. Comparison of the adsorption performance of different adsorption materials for BPA

3.5. Proposal of the comprehensive adsorption mechanism

Based on the experimental results from material structure characterization, adsorption kinetics and isotherm fitting, as well as the influence of environmental factors, this study posits that the adsorption of BPA by TFB/2-AP@sponge composites is a multi-mechanism process driven by the interplay of physical mass transfer and chemical adsorption. This process encompasses four primary mechanisms: π-π electron donor-acceptor (EDA) interactions, hydrogen bonding, electrostatic interactions, and enhanced mass transfer through multi-level channels. Each mechanism operates in concert rather than in isolation, functioning synergistically under varying pH conditions and at different stages of adsorption to facilitate the efficient and rapid removal of BPA. The following sections integrate the experimental evidence obtained and systematically elucidate the operational principles of each mechanism.

3.5.1 π-π EDA interactions

The π-π electron donor-acceptor (EDA) interaction serves as the primary driving force for the adsorption of bisphenol A (BPA) onto this material, arising from the overlap of electron clouds and the charge transfer effect between aromatic rings. The TFB/2-AP POP skeleton is rich in conjugated aromatic ring structures, while the electron-withdrawing nature of the imine bond (-C=N-) diminishes the density of the π electron cloud on the benzene ring, thereby rendering it an electron acceptor. In contrast, the two phenolic hydroxyl groups of the BPA molecule exhibit a strong electron-donating effect, which designates its benzene ring as an electron donor[38-39]. These components form stable EDA complexes through either face-to-face or edge-to-face π-π stacking. This interaction is classified as weak chemical adsorption and is characterized by high binding strength and selectivity.

Structural characterization evidence indicates the presence of abundant conjugated aromatic structures within the POP skeleton. This is supported by the vibration peaks of the aromatic ring skeleton at 1590 cm^{-1} and 1483 cm^{-1} in the FTIR spectrum, the aromatic C-H stretching vibration peak at 3061 cm^{-1}, and the characteristic aromatic carbon peak at 284.8 eV in the XPS C 1s spectrum. These findings provide a structural basis for the π-π interaction[40-41].

Adsorption model evidence reveals that the adsorption isotherms for both pure POP and composite materials align more closely with the Freundlich model ($R^2 > 0.988$). This suggests that adsorption occurs on heterogeneous surfaces and exhibits multi-layer adsorption characteristics, which is consistent with the property that π-π EDA interactions can facilitate multi-layer adsorption.

3.5.2 Hydrogen bonding interaction

Hydrogen bonding serves as a significant complement to the π-π EDA interaction, primarily occurring between the polar functional groups on the surface of POP and the phenolic hydroxyl groups of BPA. The phenolic hydroxyl group (-OH) and the nitrogen atom of the imine bond (-C=N-) present in TFB/2-AP POP function as hydrogen bond acceptors. In contrast, the hydrogen atoms of the two phenolic hydroxyl groups (-OH) in the BPA molecule act as hydrogen bond donors. This interaction results in the formation of O-H...N and O-H...O hydrogen bond networks, which further enhance the adsorption and binding strength [42-43].

The broad hydroxyl stretching vibration peak at 3403 cm^{-1}, the phenolic hydroxyl C-O stretching vibration peak at 1251 cm^{-1}, and the characteristic peak of the imine bond at 1624 cm^{-1} in the FT-IR spectrum indicate the presence of numerous hydrogen bond interaction sites on the surface of the POP [44-45]. Regarding the influence of pH, under neutral to acidic conditions with a pH range of 3 to 7, BPA predominantly exists as a neutral molecule, rendering electrostatic effects negligible. During this period, the material retains a high adsorption capacity of 150-170 $mg \cdot g^{-1}$, demonstrating that hydrogen bonds and π-π interactions collectively serve as the primary driving forces for adsorption.

3.5.3 Electrostatic Interaction (Ph-dependent mechanism)

Electrostatic interaction serves as a pH-dependent adsorption mechanism, with its intensity determined by both the surface charge of the adsorbent and the dissociation state of BPA. The pKa of BPA is approximately 9.6. At pH values less than 9.6, BPA predominantly exists as neutral molecules, while at pH values greater than 9.6, it gradually dissociates into monovalent anions (BPA^-) and divalent anions (BPA^{2-}). The imine nitrogen atoms on the surface of POP are susceptible to protonation (-CH=NH^+-) under acidic conditions, resulting in a positively charged material surface. Conversely, under strongly alkaline conditions, these

nitrogen atoms deprotonate and acquire a negative charge. When the charges of the adsorbent and BPA are opposite, electrostatic attractions occur; when they are the same, electrostatic repulsion takes place [46-47].

Experimental evidence regarding the influence of pH indicates that the adsorption capacity reaches its peak at pH 9, measuring 227.15 $mg \cdot g^{-1}$. At this pH, a portion of BPA dissociates into anions, resulting in enhanced electrostatic attraction with the positively charged surface of POP. Conversely, at pH 11, BPA is entirely dissociated into anions, and the surface of POP also acquires a negative charge due to deprotonation. This electrostatic repulsion leads to a decrease in adsorption capacity of approximately 25%. XPS characterization provides further evidence; the characteristic peak at 401.2 eV in the N 1s high-resolution spectrum corresponds to protonated imine nitrogen (-CH=NH^+-), confirming that the POP surface has undergone partial protonation in an acidic synthetic environment, thereby establishing a structural basis for electrostatic attraction [46-47].

3.5.4 Multi-level channel Mass transfer Enhancement Effect

The multi-level pore structure is essential for the rapid adsorption capabilities of POP@sponge composite materials. The hierarchical arrangement of "sponge macropores - POP mesoporous pores" significantly reduces mass transfer resistance. The three-dimensional interconnected macropores (50 μm) of the cellulose sponge serve as fluid channels, facilitating the rapid and uniform penetration of the aqueous solution to contact the loaded POP particles. Additionally, the mesoporous pores (2-50 nm) within the POP itself offer numerous active adsorption sites, thereby shortening the internal diffusion path for BPA molecules [48-49]. This structural design effectively addresses the challenges of agglomeration and the embedding of active sites in pure POP powder, thereby markedly improving the utilization efficiency of the adsorbent.

1. Evidence of morphology and pore structure: Scanning electron microscopy (SEM) images reveal that poly (phenylene oxide) (POP) particles are uniformly affixed to the surface of the sponge skeleton, without obstructing the macroscopic channels of the sponge. Brunauer-Emmett-Teller (BET) tests indicate that the material is predominantly mesoporous, exhibiting a type IV isotherm with a hysteresis loop. The pore size is compatible with that of bisphenol A (BPA) molecules (~1.0 nm), facilitating effective diffusion and adsorption [50-51].

2. Experimental evidence of adsorbent dosage: The POP@sponge composite achieves a BPA removal rate exceeding 98% at a dosage of 20 mg, which corresponds to merely 4 mg of pure POP. Furthermore, the adsorption efficiency per unit mass of POP is markedly greater than that of pure POP powder. This finding demonstrates that the sponge carrier mitigates POP agglomeration and enhances the utilization of active sites [52-53].

3.5.5 Overall verification of the synergy of multiple mechanisms

In this study, four mechanisms contributed distinctively at various stages of adsorption and under differing pH conditions, thereby establishing an efficient synergistic adsorption system. During the initial adsorption phase (0-2 h), the mass transfer advantage of multi-level channels predominated, allowing BPA molecules to swiftly access the POP surface through the sponge's macropores, exhibiting minimal resistance to liquid film diffusion and resulting in a rapid adsorption phase. In the intermediate adsorption stage (2-6 hours), π-π electron donor-acceptor (EDA) interactions and hydrogen bonding became the primary forces, facilitating

the rapid binding of BPA molecules to the active sites on the POP surface, which was characterized by a linear increase in adsorption capacity. Under weakly alkaline conditions (pH=9), electrostatic interactions synergized with π-π and hydrogen bonds, leading to the peak adsorption capacity. In the later adsorption stage (6-24 hours), multi-layer adsorption gradually approached equilibrium, causing a deceleration in the adsorption rate. A schematic summary of the proposed adsorption mechanism is shown in Figure 10.

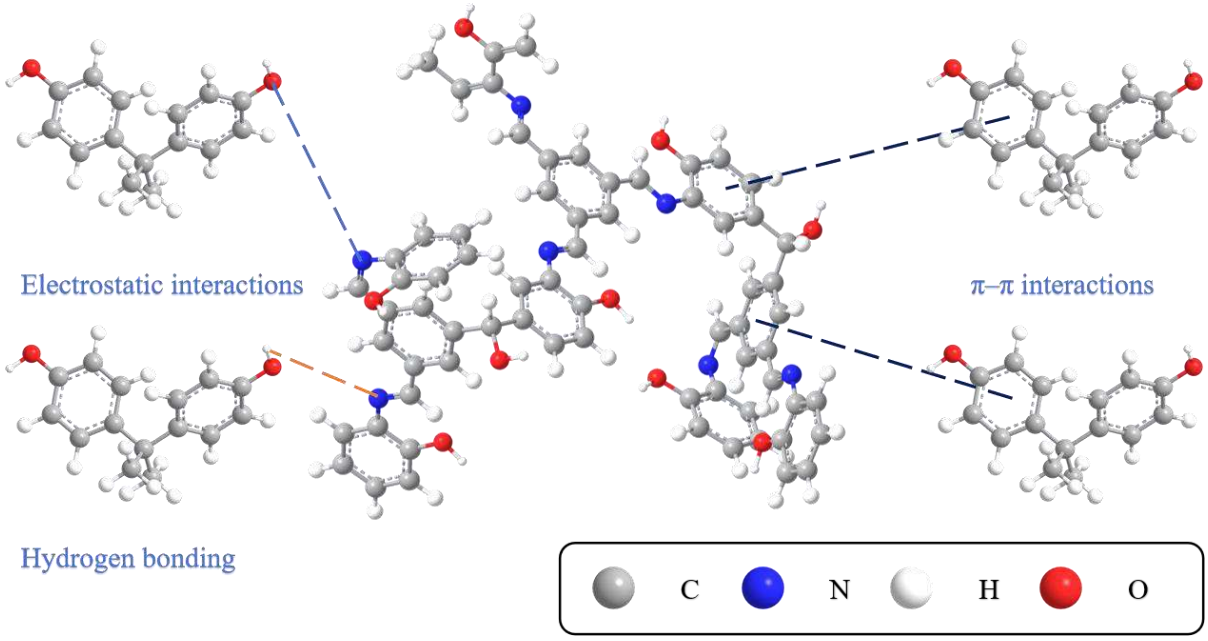


Figure 10. Schematic diagram of the mechanism of BPA adsorption by POP@sponge composite material.

4. Conclusion

In this study, we successfully synthesized an amorphous porous organic polymer based on imine bonds (TFB/2-AP POP) for the first time, utilizing 1,3,5-triformylbenzene (TFB) and o-aminophenol (2-AP) as monomers through the solvothermal method. System optimization revealed that a monomer mass ratio of 4:3 (TFB:2-AP) yielded optimal adsorption performance for bisphenol A (BPA), achieving a saturated adsorption capacity of 216.79 $mg \cdot g^{-1}$. Additionally, we constructed a macroscopic block-shaped TFB/2-AP@sponge composite material, which exhibited excellent adsorption performance and notable environmental adaptability for BPA. Under neutral conditions, the saturated adsorption capacity of the TFB/2-AP@sponge composite material remained at 171.18 $mg \cdot g^{-1}$, with a removal rate reaching 98.18% within 6 hours. Furthermore, the material demonstrated highly efficient adsorption across a wide pH range of 3 to 11, achieving an adsorption capacity of up to 227.15 $mg \cdot g^{-1}$ at pH 9, attributed to enhanced electrostatic adsorption under alkaline conditions. Characterization and mechanism analysis confirm, the adsorption of bisphenol A (BPA) is primarily facilitated by the π-π electron donor-acceptor (EDA) interaction between the aromatic ring of the porous organic polymer (POP) skeleton and BPA, alongside hydrogen bonding between the imine bond and the phenolic hydroxyl group, as well as electrostatic attraction at specific pH levels. The POP@sponge composite material developed by this research institute exhibits high adsorption capacity, rapid kinetics, broad pH adaptability, and excellent operational convenience. The use of cellulose sponge carriers not only provides the material with a macroscopic form that is easy to recycle and resistant to loss, thereby reducing operational costs and the risk of secondary pollution, but also ensures its natural degradability aligns with the principles of green and sustainable development. This material

shows significant potential for application in the treatment of wastewater containing phenolic organic pollutants, such as BPA, offering a straightforward and effective strategy for the development of high-performance nano-adsorption materials in practical water treatment initiatives.

Supplementary Information

Figure S1. **Supplementary Figure**

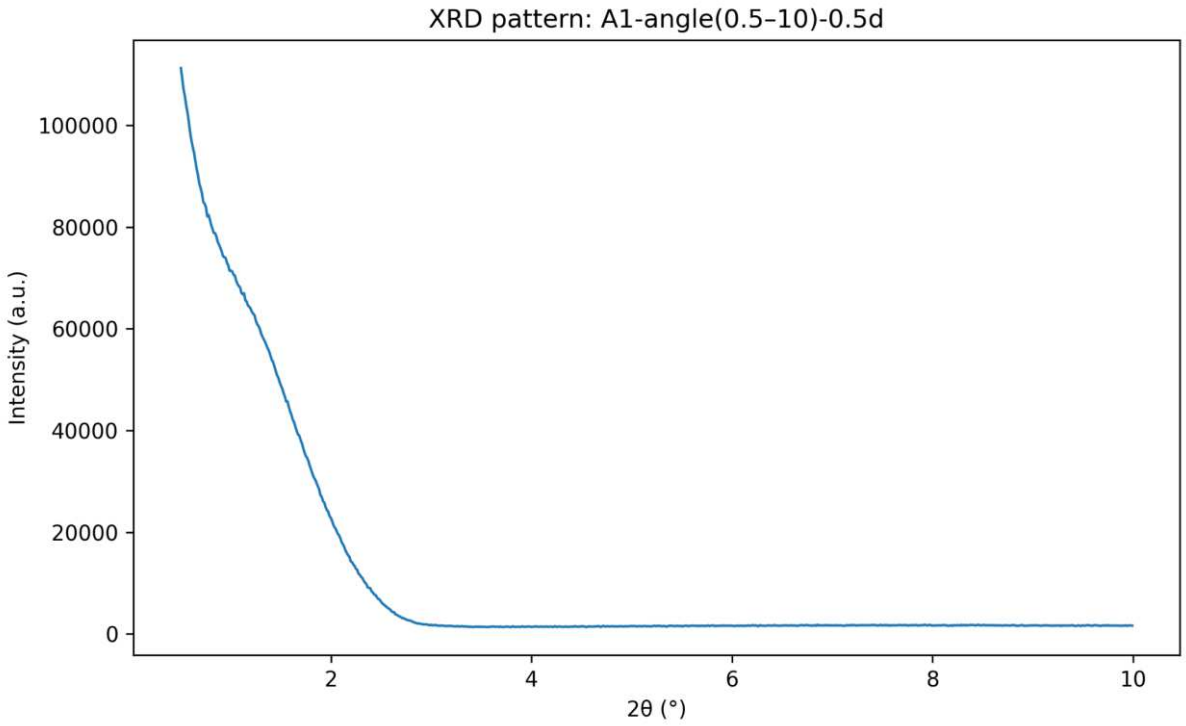


Figure S1. Low-angle X-ray diffraction (XRD) pattern of the TFB/2-AP porous organic polymer over the 2θ range of 0.5–10°.

Funding

This research received no specific grant from any funding agency in the public, commercial, or not-for-profit sectors.

References

[1] Dai, L., et al. Tuning oxygenated functional groups on biochar for water pollution control: A critical review. *J. Hazard. Mater.* **420**, 126547 (2021).

[2] Wei, T., Wu, H., Li, Z. Lignin immobilized cyclodextrin composite microspheres with multifunctionalized surface chemistry for non-competitive adsorption of co-existing endocrine disruptors in water. *J. Hazard. Mater.* **441**, 129969 (2023).

[3] Fu, D., et al. Efficient removal of bisphenol pollutants on imine-based covalent organic frameworks: adsorption behavior and mechanism. *RSC Adv.* **11**, 18308–18320 (2021).

[4] Peretz, J., et al. Bisphenol A and reproductive health: Update of experimental and human evidence, 2007–2013. *Environ. Health Perspect.* **122**, 775–786 (2014).

[5] Mustieles, V., D'Cruz, S.C., Couderq, S. A. Rodríguez-Carrillo, J.-B. Fini, T. Hofer, et al. Bisphenol A and its analogues: A comprehensive review to identify and prioritize effect biomarkers for human biomonitoring. *Environ. Int.* **144**, 105811 (2020).

[6] Cheng, F., Wang, J. Removal of bisphenol A from wastewater by adsorption and membrane separation: Performances and mechanisms. *Chem. Eng. J.* **484**, 149414 (2024).

[7] Bhatnagar, A., Anastopoulos, I. Adsorptive removal of bisphenol A (BPA) from aqueous solution: A review. *Chemosphere* **168**, 885–902 (2017).

[8] El-Sewify, I.M., Ma, S.Q. Recent developments of metal-organic frameworks for water purification. *Langmuir* **40**, 5060–5076 (2024).

[9] Kim, J.H., et al. Post-synthetic modifications in porous organic polymers for biomedical and related applications. *Chem. Soc. Rev.* **51**, 43–56 (2022).

[10] Das, S., Heasman, P., Ben, T., Qiu, S. Porous organic materials: Strategic design and structure–function correlation. *Chem. Rev.* **117**, 1515–1563 (2017).

[11] Huang, L., et al. Nanoarchitectured porous organic polymers and their environmental applications for removal of toxic metal ions. *Chem. Eng. J.* **408**, 127991 (2021).

[12] Cooper, A.I. Porous organic polymers. *Chem. Soc. Rev.* **40**, 18–39 (2011).

[13] Zhang, R., et al. Porous polymer adsorbents of tris(4-formylphenyl)amine and β-cyclodextrin for endocrine-disrupting chemicals, dyes, and antibiotics. *ACS Appl. Polym. Mater.* **8**, 2831–2845 (2026).

[14] Zhao, X., Liu, Y., Zhu, Q., Gong, W. Catechol-based porous organic polymers for effective removal of phenolic pollutants from water. *Polymers* **15**, 2565 (2023).

[15] Wei, D., et al. Understanding bisphenol-A adsorption in magnetic modified covalent organic frameworks: Experiments coupled with DFT calculations. *J. Mol. Liq.* **301**, 112431 (2020).

[16] Zhang, M., et al. Hierarchical-coassembly-enabled 3D-printing of homogeneous and heterogeneous covalent organic frameworks. *J. Am. Chem. Soc.* **141**, 5154–5158 (2019).

[17] Li, N., et al. Porous organic polymers for superefficient removal of pollutants from water: Design, synthesis and adsorption performance. *J. Clean. Prod.* **396**, 136558 (2023).

[18] Wang, G., et al. A cellulose sponge with robust superhydrophilicity and under-water superoleophobicity for highly effective oil/water separation. *Green Chem.* **17**, 3093–3099 (2015).

[19] Hoo, D.Y., et al. Ultrasonic cavitation: An effective cleaner and greener intensification technology in the extraction and surface modification of nanocellulose. *Ultrason. Sonochem.* **90**, 106176 (2022).

[20] Carrington, M.E., et al. Sol-gel processing of a covalent organic framework for the generation of hierarchically porous monolithic adsorbents. *Chem* **8**, 2961–2977 (2022).

[21] Fenton, J.L., Burke, D.W., Qian, D. M. Olvera de la Cruz, W.R. Dichtel, Polycrystalline covalent organic framework films act as adsorbents, not membranes. *J. Am. Chem. Soc.* **143**, 1466–1473 (2021).

[22] Liu, X., et al. Binder-free 3D printing of covalent organic framework (COF) monoliths for CO2 adsorption. *Chem. Eng. J.* **403**, 126333 (2021).

[23] Thommes, M., et al. Physisorption of gases, with special reference to the evaluation of surface area and pore size distribution (IUPAC Technical Report). *Pure Appl. Chem.* **87**, 1051–1069 (2015).

[24] Beamson, G., Briggs, D. *High Resolution XPS of Organic Polymers: The Scienta ESCA300 Database*. John Wiley & Sons, New York (1992).

[25] Wang, J., Guo, X. Adsorption kinetic models: Physical meanings, applications, and solving methods. *J. Hazard. Mater.* **390**, 122156 (2020).

[26] Foo, K.Y., Hameed, B.H. Insights into the modeling of adsorption isotherm systems. *Chem. Eng. J.* **156**, 2–10 (2010).

[27] Feriante, C., et al. New mechanistic insights into the formation of imine-linked two-dimensional covalent organic frameworks. *J. Am. Chem. Soc.* **142**, 18637–18644 (2020).

[28] Grenier-Loustalot, M.-F., Larroque, S., Grenier, P., Leca, J.-P., Bedel, D. Phenolic resins: 1. Mechanisms and kinetics of phenol and of the first polycondensates towards formaldehyde in solution. *Polymer* **35**, 3046–3054 (1994).

[29] Gong, L., Zhu, H., Wu, W., Lin, D., Yang, K. A durable superhydrophobic porous polymer coated sponge for efficient separation of immiscible oil/water mixtures and oil-in-water emulsions. *J. Hazard. Mater.* **425**, 127980 (2022).

[30] Liu, Z., Wang, H., Ou, J., Chen, L., Ye, M. Construction of hierarchically porous monoliths from covalent organic frameworks (COFs) and their application for bisphenol A removal. *J. Hazard. Mater.* **355**, 145–153 (2018).

[31] Fang, Y., et al. Hierarchical covalent organic frameworks-modified diatomite for efficient separation of bisphenol A from water in a convenient column mode. *Sep. Purif. Technol.* **298**, 121611 (2022).

[32] Li, X., Zhou, M., Jia, J., Ma, J., Jia, Q. Design of a hyper-crosslinked β-cyclodextrin porous polymer for highly efficient removal toward bisphenol A from water. *Sep. Purif. Technol.* **195**, 130–137 (2018).

[33] Zhuang, Y., Li, S., Rene, E.R., Dong, S., Ma, W. Green synthesis of magnetic azo-linked porous organic polymers with recyclable properties for enhanced Bisphenol-A adsorption from aqueous solutions. *Environ. Res.* **249**, 118427 (2024).

[34] Li, Z., Hu, C., Hu, Z., Fu, Y., Chen, Z. Facile synthesis of novel multifunctional β-cyclodextrin microporous organic network and application in efficient removal of bisphenol A from water. *Carbohydr. Polym.* **276**, 118786 (2022).

[35] Bhadra, B.N., Lee, J.K., Cho, C.-W., Jhung, S.H. Remarkably efficient adsorbent for the removal of bisphenol A from water: Bio-MOF-1-derived porous carbon. *Chem. Eng. J.* **343**, 225–234 (2018).

[36] Lee, M.Y., et al. Aqueous adsorption of bisphenol A over a porphyrinic porous organic polymer. *Chemosphere* **265**, 129161 (2021).

[37] Dong, S., Rene, E.R., Zhao, L., Xiaoxiu, L., Ma, W. Design and preparation of functional azo linked polymers for the adsorptive removal of bisphenol A from water: Performance and analysis of the mechanism. *Environ. Res.* **206**, 112601 (2022).

[38] Wang, Y., Wang, W., Zhang, Z., Li, P. Adsorption performance of the functional COFs for removal of bisphenol A: Molecular dynamic simulations. *J. Mol. Liq.* **392**, 123475 (2023).

[39] Xiong, M., et al. Probing the adsorption behavior and mechanism of NO2 and NH2 functionalized covalent organic frameworks (COFs) for removal of bisphenol A. *Microporous Mesoporous Mater.* **346**, 112299 (2022).

[40] Lai, Y., et al. Efficient adsorption of bisphenol A by metal-organic frameworks-derived N-doped carbon nanoflakes: Adsorption performance and mechanism investigation. *Sep. Purif. Technol.* **325**, 124748 (2023).

[41] Zhao, Y., Feng, C., Tian, C., Li, Z., Yu, Y. Enhanced adsorption selectivity of bisphenol analogues by tuning the functional groups of covalent organic frameworks (COFs). *Sep. Purif. Technol.* **297**, 121489 (2022).

[42] Liu, J., et al. Concurrent elimination and stepwise recovery of Pb(II) and bisphenol A from water using β-cyclodextrin modified magnetic cellulose: adsorption performance and mechanism investigation. *J. Hazard. Mater.* **432**, 128758 (2022).

[43] Chen, Z.-H., et al. β-Cyclodextrin-modified graphene oxide membranes with large adsorption capacity and high flux for efficient removal of bisphenol A from water. *J. Membr. Sci.* **595**, 117510 (2020).

[44] Zhong, X., Lu, Z., Liang, W., Hu, B. The magnetic covalent organic framework as a platform for high-performance extraction of Cr(VI) and bisphenol A from aqueous solution. *J. Hazard. Mater.* **393**, 122353 (2020).

[45] Wei, X., Wei, Q., Liu, H. Tailored covalent organic frameworks with tunable fluorine groups for efficient adsorption of bisphenol analogues. *J. Hazard. Mater.* **513**, 142433 (2026).

[46] Teramoto, K., Harada, T., Sakohara, S. Adsorption of bisphenol-A by pH-responsive polymer grafted on porous polyethylene vinyl acetate disk: Effect of the side-chain length of hydrophobic component in polymer on adsorption. *Chem. Eng. J.* **258**, 386–393 (2014).

[47] Ahmed, M.B., Zhou, J.L., Ngo, H.H., Johir, M.A.H., Sornalingam, K. Sorptive removal of phenolic endocrine disruptors by functionalized biochar: Competitive interaction mechanism, removal efficacy and application in wastewater. *Chem. Eng. J.* **335**, 801–811 (2018).

[48] Zhou, L., et al. Efficient adsorption of bisphenol A from water by a hierarchically porous hyper-crosslinked polymer containing β-cyclodextrin polyurethane. *Sep. Purif. Technol.* **319**, 124076 (2023).

[49] Wang, L., et al. Electrocleavage synthesis of solution-processed, imine-linked, and crystalline covalent organic framework thin films. *J. Am. Chem. Soc.* **144**, 8961–8968 (2022).

[50] Wu, D., et al. Design and preparation of porous polymers. *Chem. Rev.* **112**, 3959–4015 (2012).

[51] Geng, K., et al. Covalent organic frameworks: Design, synthesis, and functions. *Chem. Rev.* **120**, 8814–8933 (2020).

[52] Lv, Y., et al. Rapid elimination of trace bisphenol pollutants with porous β-cyclodextrin modified cellulose nanofibrous membrane in water: adsorption behavior and mechanism. *J. Hazard. Mater.* **403**, 123666 (2021).

[53] Jiang, X., et al. In-situ growth of olefin-linked covalent organic framework nanofiber membranes via surface-mediated condensation for sustainable removal of bisphenol A. *J. Hazard. Mater.* **494**, 138616 (2025).